CHAPTER 7

STRUCTURAL CHACTERISATION OF VIGODI-GUGRIANA-KHIRASRA-NETRA FAULT SYSTEM (VGKNFS)

The neotectonically active KRB has undergone thick-skinned deformation and represent positive basin inversion tectonics. So as to define the major and minor stress fields reliably and to understand the effect of local perturbations in the regional stress field acting upon the VGKNFS, unnamed cross-faults of varying orientations are also included in the paleostress analysis, along with the major NW striking faults. The structural data collected from the western part of the KMF are not included in the paleostress analysis. The KMF is mainly non-striated and acts as a lithotectonic contact between Mesozoic rocks and Tertiary rocks. Since the KMF is non-striated, the collected structural measurements will be incomplete for paleostress analysis to be conducted and paleostress analysis findings would be presented with a low confidence interval.

The KMU is sub-divided into four structural zones – the NHRFZ along the KMF, KHRFZ along the KHF, VGKNFS and Bhuj structural low (Fig. 7.1) (Biswas, 1993). E-W striking, intra-basinal faults are affected and segmented by N, NW, NE, NNW and NNE striking, m to km-scale, transverse faults with dip-/oblique-slip deciphered in the field (Biswas, 1993; Maurya et al., 2003). The NW striking VGKNFS, which formed during the basin rift phase, is traceable for ~80 km with a fault zone width of ~10 km. Being located between E-W striking NHRFZ and KHRFZ at western part of KMU, the VGKNFS is affected by NW striking, essentially dip-slip faults (Fig. 7.1) (Biswas, 1993).

The aim of the present study is to understand the temporal and spatial evolution of the acting stress field. The existence of two end-member phases of deformation that prevailed since the Mesozoic from extension to compression is discussed. Kinematic analysis of brittle structures is performed that provides insights to relate the evolution of faults with the prevalent regional tectonic stress conditions that (re)activated the faults. Inversion of fault-slip data gives the orientation of principal stress axes. Knowledge of the present-day stress field is critical for seismic hazard estimation and mitigation. Also, it is equally important to understand the paleostress field operating at

the time of faulting to reconstruct the tectonic evolution of faults in the KRB. The state of tectonic stress can be inferred from the geological and geophysical data e.g., inversion of earthquake Focal Mechanism Solution (FMS), borehole breakouts (BO), drilling-induced fractures, in-situ stress measurements (overcoring and hydraulic fracturing), geological indicators (fault-slip data, volcanic vent alignments) (Zoback, 1992). These provide an accurate estimate of the prevalent paleostress as well as preset-day stress conditions. No attempt has been made so far to reconstruct the paleostress state using geological indicators and to understand the kinematics and brittle tectonics of the KRB. Notably, Vanik et al. (2018) has carried out paleostress analysis using geological indicators along the E striking Katar fault from SW Saurashtra region of Gujarat state, which is ~370 km S of the study area and may not have direct implications.

The technique of stress-inversion is a relatively recent but now classical approach used in seismotectonics to infer crustal stress from earthquake focal structures and from geological fault-slip evidence and related slip lines in brittle tectonics. Fault-slip data as kinematic markers used in paleostress reconstruction allows local to regional scale heterogeneous, multiphase geodynamic reconstructions. To determine the orientation of principal stress axes, a large number of measured meso-scale faults and their associated slip indicators (fault-slip data) are needed This necessitates the rocks exposing faults with enough slip/data along a broad range of shear plane orientations, so that the size of each individual brittle structure must be lower than the sampled volume (Angelier, 1994). The W–NW striking KMF acts as a lithotectonic contact between the rocks of Mesozoic Formation in the upthrown block and Tertiary Formation in the downthrown block. In the western part of the KMF, no outcrop is found exposing the striated plane of the KMF. Therefore, it was not possible to collect fault-slip measurements and to observe the kinematic indicators, which are the prerequisite for carrying out the paleostress analysis. The studies are mainly focused in the VGKNFS, which is located south of the KMF. The VGKNFS exposes variably oriented faults in uniform lithology with plenty of exposures of striated fault planes.

GEOLOGICAL AND STRUCTURAL SETTING

The greatest uplift in the KRB, the KMU consists of several deformation zones as stated earlier. Out of them, the NW striking VGKNFS is one such major brittle shear zone located in the western part of KMU (Biswas, 2016). The tectonically active eastern

zone of KMU is separated from its tectonically stable western counterpart by the VGKNFS (Biswas, 1993). The VGKNFS is categorized as an intra-uplift fault system as it is located within the KMU and also to differentiate it from the uplift-bounding fault systems of the KRB, e.g., the KMF. Around 80 km long VGKNFS exposes the (sub-)parallel strands of step faults: *(i)* NW striking, ~50 km long Vigodi Fault (VF) and its bifurcation; NNW striking, ~7.15 km long West Vigodi Fault (WVF); *(ii)* NW striking, ~45 km long, Gugriana Fault (GUF) with bifurcations; NNW striking, ~10 km long Khirasra Fault (KF); and NW striking, ~8 km long North Khirasra Fault (NKHF); and *(iii)* NNW striking, ~13 km long Netra Fault (NF) (Fig. 7.1). Besides, there are numerous NW, NE and E striking cross-faults. NW striking faults are more numerous than the NE striking faults and, NNW and E striking faults are few.

The study area falls in the Survey of India (SOI) topographic sheet numbers 41E/2, 41E/3 and 41A/14 at 1:50,000 scale. Since the study area is vast (~150 km^2 stretch), the ~80 km long VGKNFS is divided into four sectors. This separation into sectors is necessary to investigate the spatial variation in paleostress field and also to understand the change in kinematic behavior of cross-faults of varying orientations exposed in the entire study area (Fig. 7.1). The boundaries of these four sectors are fixed based on the structural continuity of major NW striking faults in the VGKNFS determined during extensive field structural investigations (Fig. 7.1).

The VGKNFS exposes SW dipping major faults showing asymmetric tectonic uplift on their upthrown side, producing a 7-10 km wide, NW striking narrow flexure zone. The VGKNFS is terminated by an E-ESE striking, ~193 km long NHRFZ on its northern extremity and E striking, ~65 km long KHRFZ on its southern extremity. Thus, the VGKNFS makes an acute angle (50-70°) with the uplift-bounding faults (Biswas, 1993). Faults network dies out to the southern margin of Ghuneri dome, Mundhan anticline and Jara dome of the NHRFZ.

The length and amount of slip of faults in the VGKNFS are much less than the E striking uplift-bounding faults viz., the KMF. The VGKNFS occurs mainly in Mesozoic outcrops affecting the Jhuran and Bhuj Formation consisting dominantly of sandstones and shales with limestones. Faults are also reported to be exposed in the Deccan Trap flows (Biswas, 1993). NE, NNE, N, ENE and E striking secondary faults are often accompanied by dykes in the central and eastern parts of KMU (Biswas, 1993). However, in the western part of KMU, in the study area, VGKNFS is devoid of any dykes except the ~E striking Ukra intrusive to the south of NHRFZ (Biswas, 1993)

(Fig. 7.1). These faults are pre-Tertiary as the VGKNFS neither affects ~E striking Tertiary belt of KMU to south of the Deccan Trap nor in other areas of Tertiary exposures (Biswas, 1993).

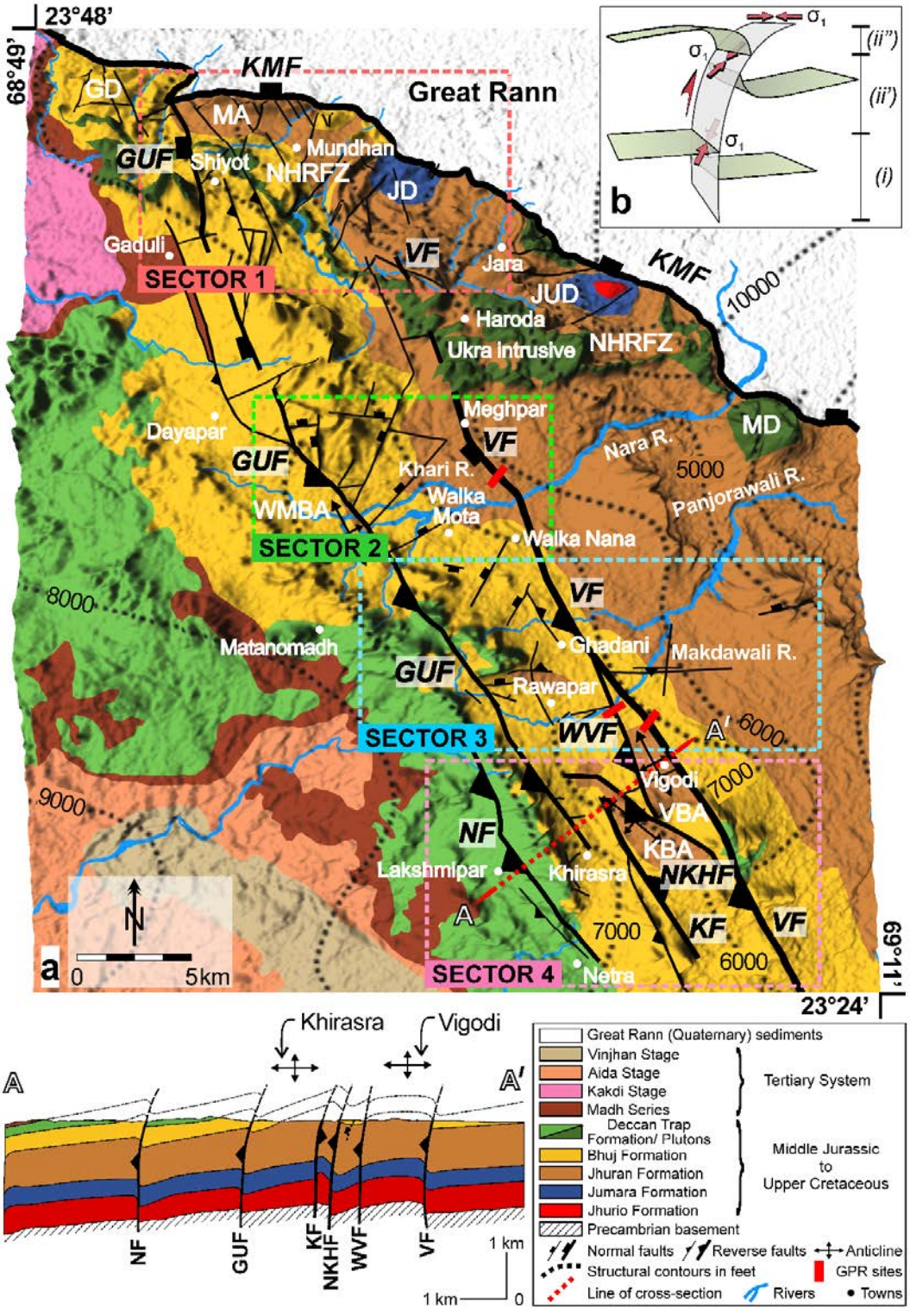

Fig. 7.1. (a) Tectonic scheme of the VGKNFS as mapped in the present study, after Shaikh et al. (2020). The structural contours with 1000 feet (values are in negative) contour interval are drawn over the top of Precambrian basement. The schematic cross-section A–A$^{/}$ below the map is redrawn from Biswas (1993). VF: Vigodi Fault, WVF: West Vigodi Fault, GUF: Gugriana Fault, KF: Khirasra Fault, NKHF: North Khirasra Fault, NF: Netra Fault, KMF: Kachchh Mainland Fault, NHRFZ: Northern Hill Range Fault Zone, VBA: Vigodi Brachy-Anticline, KBA: Khirasra Brachy-Anticline, WMBA: Walka Mota Brachy-Anticline, GD: Ghuneri dome, MA: Mundhan Anticline, JD: Jara Dome, JUD: Jumara Dome and MD: Manjal Dome. (b) Depth profile of upthrust fault modified and redrawn after fig. 5 of Prucha et al. (1965). Red, inward-pointed double arrows indicate depth-wise rotation in the orientation of maximum principal stress axis (σ_1).

NW-NNW striking VF (60-80° dip) is the longest and the easternmost fault of VGKNFS (Fig. 7.1). The throw of VF is estimated to be 45-61 m (Biswas, 1993). The discontinuous NW-NNW striking GUF originates in the saddle region between the Ghuneri dome and Mundhan anticline (Fig. 7.1). The GUF dips 60-85° towards SW with the maximum throw is around the locality Gugriana. NW-NNW striking KF and NKHF are the branches of GUF extending to the SE (Biswas, 1993) (Fig. 7.1). The NNW-NW striking NF is dipping 70-75° towards the upthrown SW side. The NF is of post-Paleocene in age (Biswas, 1993). NW striking VGKNFS is also riddled with a network of NE, NW and E striking small-scale, unnamed cross-faults (Fig. 7.1). They run for tens of meters to few kms and then die out/truncate in the deformation zone of NW striking major faults.

Basement-controlled tectonics has shaped out the present geometry of VGKNFS (Prucha et al., 1965; Biswas, 1993). All the four major fault strands are basement faults. They act as plunging upthrust due to their differential vertical uplift along the entire length of the individual fault strands (Fig. 7.1b). The fault geometry is deduced based on the present structural studies and geological work carried out by Biswas (1993). The geometry and attitude of upthrust faults change depth-wise in the sense that they are *(i)* initially vertical/near-vertical at depth, but becomes *(ii)* convex upward with reverse slip (anti-listric) as they grow upward, and eventually rotate toward the downthrown block (Miller and Mitra, 2011). The upthrust faults also show drape-folding of sedimentary units over the displaced basement rocks.

Methods

To understand the kinematic evolution of VGKNFS, detailed structural analysis at regional scale was carried out.

(i) paleostress analysis using collected fault-slip data,

(ii) statistical analysis using derived compressional stress directions of major and unnamed cross-faults.

PALEOSTRESS ANALYSIS

Paleostress analysis is now a well-practiced technique that has widespread consideration in order to understand different tectonic events (Federico et al., 2014; Giambiagi et al., 2017; Vanik et al., 2018; Goswami et al., 2020). The results are represented in the form of a paleostress tensor made up of three mutually perpendicular principal stress axes, viz. the maximum principal stress axis (σ_1), intermediate principal stress axis (σ_2) and minimum principal stress axis (σ_3); and the stress ratio (R). The parameter $R = (\sigma_2 - \sigma_3)(\sigma_1 - \sigma_3)^{-1}$ defines the shape of stress ellipsoid (Angelier, 1994; Delvaux et al., 1997; Lahiri et al., 2020). Furthermore, the orientation of the maximum and minimum horizontal principal stress (S_{Hmax} and S_{hmin}) are indicated.

Spatially or temporally varying stress regime may work on the same fault plane. Temporally, the fault may reactivate multiple times preserving several mutually superimposed striations orientations. Alternatively, the fault may show spatial variation in the stress orientations. Such fault-slip data are called heterogeneous (Yamaji and Sato, 2019). Multiple stress states are required to explain the heterogeneous fault-slip data. Fault-slip data are called homogeneous if a single stress state explains the whole fault-slip dataset (Yamaji and Sato, 2019).

The fault-slip data comprising of attitude of fault planes and slickenside lineations are measured. The slip-sense of faults was determined by observing various slickenside kinematic indicators. To accurately compute the paleostress state belonging to distinct tectonic events, to minimize the uncertainties and to cross-examine and increase the reliability of results, several open-source computer programmes were used that work with different procedures, viz., Win_Tensor (v.5.8.8) (Delvaux and Sperner, 2003), T-Tecto studio X5 (Zalohar and Vrabec, 2007), FaultKin (v.8.0) (Marrett and Allmendinger, 1990; Allmendinger et al., 2012) and SG2PS (Sasvári and Baharev, 2014) (Appendix-A for working principles). Several attempts have been made to analyze and compare the results of paleostress analysis performed using multiple

algorithms on natural datasets (Sippel et al., 2009; Federico et al., 2014; Vanik et al., 2018; Maestro et al., 2018). Using the aforementioned four programmes, three types of brittle structures were incorporated in the procedure: *(i)* fault planes with slickenside lineations, *(ii)* deformation bands with striated, principal slip surface, and *(iii)* systematic joints. In the fault damage zone, it is assumed that the tilting of beds is presumably synchronous to faulting. Negligible tilt of beds is observed in the narrow deformation zone, therefore, there was no need to un-tilt the bedding from the resultant paleostress tensors.

Fundamental assumptions

Paleostress analysis presumes several points (Etchecopar et al., 1981; Simón, 2019). *(i)* As per the Wallace-Bott hypothesis, fault plane slips in the direction of maximum resolved shear stress (τ_{max}) (Wallace, 1951; Bott, 1959). This assumption holds true as it is exemplified by a rather small percentage of fault-slip data showed the misfit angle $\geq 20°$. *(ii)* Slip failure occurs in homogeneous and isotropic rock bodies. *(iii)* Stress field is spatially and temporally homogeneous (Kaven et al., 2011). In order to accomplish this assumption, fault-slip measurements were collected from each of the sites and data were not mixed from different sites. Only long, straight, parallel oriented striations indicative of stress homogeneity were measured and included in the dataset. *(iv)* Slip occurs on faults of varied orientations and thus, faults are not necessarily oriented in the optimum direction with respect to the principal stresses as predicted from Coulomb failure criterion (Twiss and Unruh, 1998). *(v)* The rock volume experiencing faulting is large compared to the scale of faults and displacement along the faults is small compared to fault dimensions (Simón, 2019). In order to fulfil this assumption, sufficient number of fault-slip data were collected from each of the sites.

Slickenside kinematic indicators

As the fault planes are exposed in uniform lithology, the sense of slip cannot be determined due to lack of any offset markers. In such cases, the slip-sense was inferred solely by observing various slickenside kinematic indicators following the detail works of Doblas et al. (1997), Doblas (1998) and Petit (1987). Multiple types of kinematic indicators were noted from the fault plane at each site in order to assure the sense of slip. V-shaped crescentic markings include debris trails, sheltering trails, carrot-shaped gouging-grain grooves (Doblas, 1998). Mineral steps include fault plane asperities (or

spurs), quartz crystal fibers, knobby elevations, detached and trailed fragments and tension gashes sub-perpendicular to orientation of striations (Doblas et al., 1997; Doblas, 1998). Nearly all fault planes follow the positive smoothness criteria (i.e., smoothness feels in the direction of motion of missing block) with few follow negative smoothness criteria. Linear, pipe-shaped and v-shaped gouging-grain grooves generated due to trailed material were also observed (Doblas, 1998). Asymmetric depressions due to removed fault plane material during frictional movement were also observed (Doblas, 1998). Trains of inclined planar structures include domino-style offsetting in tilted blocks exposed in either the footwall or hangingwall; multiple, secondary, synthetic, striated slip surfaces associated with the principal, striated slip surface. Drag effect of planar elements includes normal and reverse drag. These features are associated with the principal slip surface. They were also used to decode the slip-sense (Doblas, 1998; Mukherjee, 2014). Secondary fractures with diverse morphological variation developed on the fault plane, for example, those following the T-criteria (riedel shear fractures): tensile and crescentic fractures; R-criteria (secondary, synthetic, striated, shear fractures of R orientation): RO-type, RM-type and lunate fractures; P-criteria (secondary, striated, shear fractures of P orientation): PT-type and PO-type were found useful (Petit, 1987). The morphology of each of the slickenside kinematic indicator is discussed in detail in the field investigations and fault-slip analysis results.

FIELD INVESTIGATIONS AND FAULT-SLIP ANALYSIS RESULTS

In the VGKNFS, nearly all fault planes of different trends dip steeply (55-88°, few < 55°). NW striking major faults dip uniformly towards SW resembling step-like pattern. Sharp (sub-)vertical steepening of beds of Jhuran and Bhuj sandstones mark the presence of faults. The faults stand out as hard, resistant, positive relief structures against the eroded flat plains and are clearly noticeable from a distance. Straight fault lines with prominent topographic expression can also be observed in Google Earth Pro imageries (e.g., site 71). This exercise allowed us to define the continuity of major and other unnamed cross-faults. Long, discontinuous, prominent narrow ridges striking parallel to faults, steep escarpment face and sharp bend of streams are some of the prominent geomorphic expressions that helped in locating the faults. Throw above the ground surface ranges 0.5-30 m. Despite their lower stratigraphic offset than that of E striking uplift-bounding faults, the VGKNFS crops out discontinuously occurring faults

for tens of kms. Along strike, maximum throw is observed around the central part, in Khirasra-Vigodi region, which decreases away towards both the ends of faults and continues as only few m high, discontinuously occurring fault plane above the ground surface.

Each of the sector described earlier comprises variably oriented (NW-NNW, NNE-NE and E) striated and non-striated fault surfaces. *(i)* Northernmost sector 1 (number of collected fault-slip data (nt) = 129) comprises 08 sites, which are included in fault-slip analysis. The sites are located at northern extremity of NW striking GUF, VF; and also other NE, NNE and NW striking unnamed faults originating in the NHRFZ (from Mundhan anticline, Jara dome and inter-domal saddle region in between these two structural domes). *(ii)* South of the Haroda pluton, sector 2 (nt = 463) is located, far away from the influence of NHRFZ. 21 sites are included in fault-slip analysis from sector 2. NW striking GUF; NE, NNE and E striking unnamed faults mostly terminating in the deformation zone of GUF are exposed in sector 2. Also included is the NNW striking rotational VF with anticlockwise rotation of the fault plane (dip direction changing from SW to NE). Fault-slip data are collected from both SW and NE dipping VF. *(iii)* Sector 3 (nt = 443) includes 29 sites exposing NW striking GUF and VF, and NNW striking WVF. NW, NE, E striking, striated/non-striated, unnamed faults and deformation band faults are also included in sector 3. *(iv)* From W to E, sector 4 (nt = 115) includes 08 sites exposing NW striking NF; southernmost extremity of NW-NNW striking GUF; bifurcations of the GUF: NW striking NKHF and NNW striking KF. Further E, NW striking VF; and few NW, NNW and E striking unnamed non-striated faults are exposed. VF and GUF are exposed in all the four sectors; WVF is exposed in sector 3 and 4; NKHF and KF in sector 4 only; and NF in sector 3 and 4 (Fig. 7.1).

Mostly dip-slip striations were observed at almost all the sites, which essentially mark normal/reverse slip. Fault planes exposing striations with horizontal/sub-horizontal plunge that record dextral or sinistral slip were scanty. Therefore, fault-slip data indicating strike-slip motion were not included in paleostress analysis. Total 100 sites were explored where fault planes are exposed, out of which 66 sites (including one with systematic joints) were incorporated in paleostress analysis. The remaining 34 sites consist of non-striated fault surfaces, and were excluded from fault-slip analysis.

In VGKNFS, most of the faults show plastered, polished, corrugated and slickensided slip planes affected by (sub-)parallel or conjugate shear fractures.

However, at few sites, fault planes are covered by dense, hard, dark reddish ferruginous fault gouge or breccia. No striated slip surface was observed at such sites. Non-striated faults (sense-only data), faults with poor slickenside lineations and unknown slip-sense (line-only data) – fall under the not sure category of fault-slip data (Yamaji and Sato, 2019). Although, paleostress analysis programmes provide handling of such dataset, they were not included in the analysis (Sperner and Zweigel, 2010). Only faults with known or confidently inferred slip-sense were incorporated. Few sites (e.g., site 4 along GUF and site 44 along VF) show development of quartz slickenfibers indicating creep along the fault plane. The faults were studied in vertical/oblique-sections, in the vicinity of anticlines and synclines, sometimes exposed in the riverbed or on a relatively flat topography.

SECTOR 1

Two major structures: the Mundhan anticline and Jara dome are exposed in sector 1, generated due to periodic tectonic movement along W-NW striking KMF (Fig. 7.2).

The NW end of VGKNFS is exposed in sector 1 where the identity of NW striking major faults is lost among NW and NE striking discontinuous faults across the Mundhan anticline and Jara dome (Figs. 7.1, 7.2). Node and branch topology network in map-view can be very well expressed as NW striking faults are the younger ones and more extensive that truncate the pre-existing NE striking faults forming characteristic Y-pattern (Morley and Nixon, 2016). In the northernmost extremity, both, NW and NE striking faults disappear in the deformation zone of the KMF (Fig. 7.2).

Vigodi Fault (VF) with reverse slip

NW striking and SW dipping VF is encountered in Jhuran sandstone at site 16 (sector 1, Fig. 7.2). The site crops out the northernmost exposure of VF. Further NW, the fault dies out in the SW fringe of Jara dome. It does not pass through the E-W striking Jaramara scarp located south of Jara dome. Fault-slip analysis results indicate that the VF at site 16 has experienced reverse slip with NE oriented fault-perpendicular shortening (Appendix-B).

~3 km east of Lakhapar, in its NW extremity, the VF exposes in the Jhuran sandstone near SW fringe of the Jara dome, ~1 km south of the E trending Jaramara scarp. Further NW, the VF disappears among several NE and NW trending faults in the

southern fringe of the Jara dome. Towards SE, the VF, then, disappears within the WNW trending Haroda pluton. Further SE, the VF reappears within the Jhuran sandstone and then, is exposed in Bhuj sandstone SE of Walka Nana.

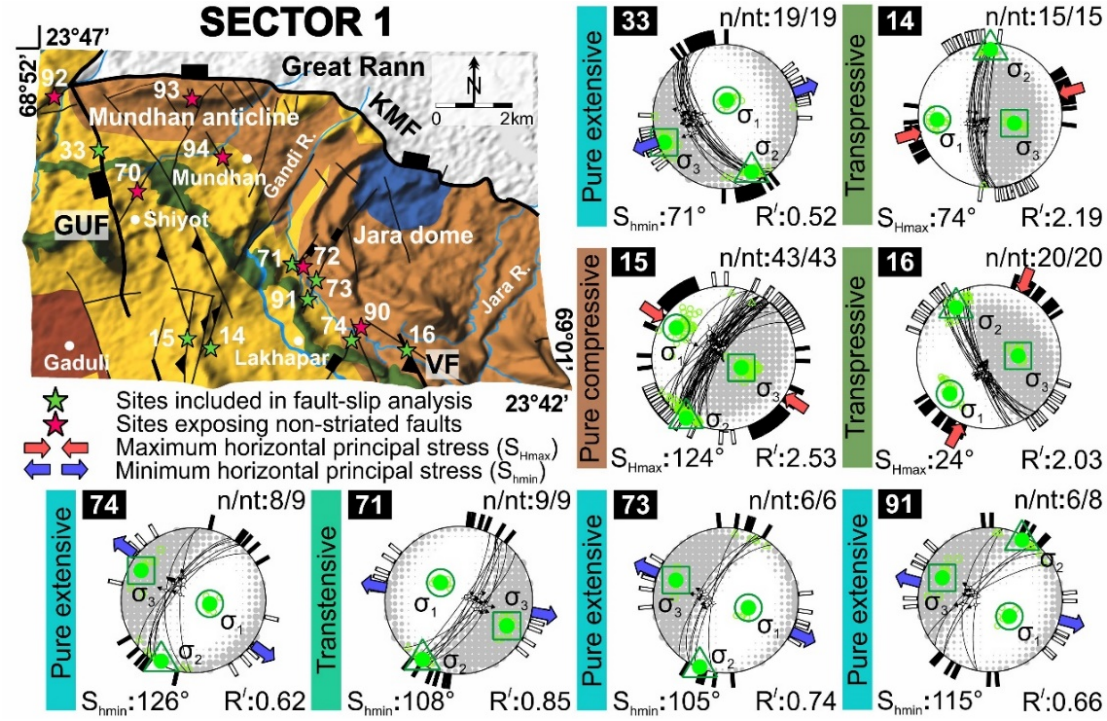

Fig. 7.2. Structural map of sector 1 (location shown in the geological map of study area in Fig. 7.1). The sites of fault-slip measurements are marked by green stars. The sites exposing non-striated faults are marked by red stars and are not included in fault-slip analysis. Follow Fig. 7.1 for interpretation of colors related to lithology shown in the structural map. The stress tensors (lower hemisphere, equal-area projection) deduced by Right Dihedral Method (RDM) implemented in Win_Tensor (Delvaux and Sperner, 2003) for respective sites are shown. Black lines: fault planes with slip vectors (marked by open circles with arrows). Red inward-pointed and blue outward-pointed double arrows: orientation of maximum (S_{Hmax}) and minimum (S_{hmin}) horizontal principal stress respectively. Green circle, triangle and square: orientation of maximum (σ_1), intermediate (σ_2) and minimum (σ_3) stress axes respectively ($\sigma_1 \geq \sigma_2 \geq \sigma_3$). Black solid bars and open bars at the periphery of paleostress tensors: orientation of S_{Hmax} and S_{hmin} axes respectively, for individual fault-slip data. For normal faults, $S_{hmin} = \sigma_3$ and for reverse faults, $S_{Hmax} = \sigma_1$. Site numbers are shown on upper left of stereoplots. n/nt: ratio of number of fault-slip data used in paleostress analysis relative to the total number of fault-slip data collected from the specific site. R': stress index (Delvaux et al., 1997). Counting grid: the white and grey quadrants of the stereoplots corresponding to regions of compression and tension respectively. The colored panels on left of each stereoplots represent the inferred stress regime.

Gugriana Fault (GUF) with oblique-slip

In sector 1, NW striking GUF crops out only at site 33, ~2 km south of western flank of the Mundhan anticline (Fig. 7.2). The present site witnesses the northernmost occurrence of GUF in Bhuj sandstone. Further north, the fault disappears in the damage zone of KMF. GUF may be a branch of the KMF. Further field investigations are required to verify this statement.

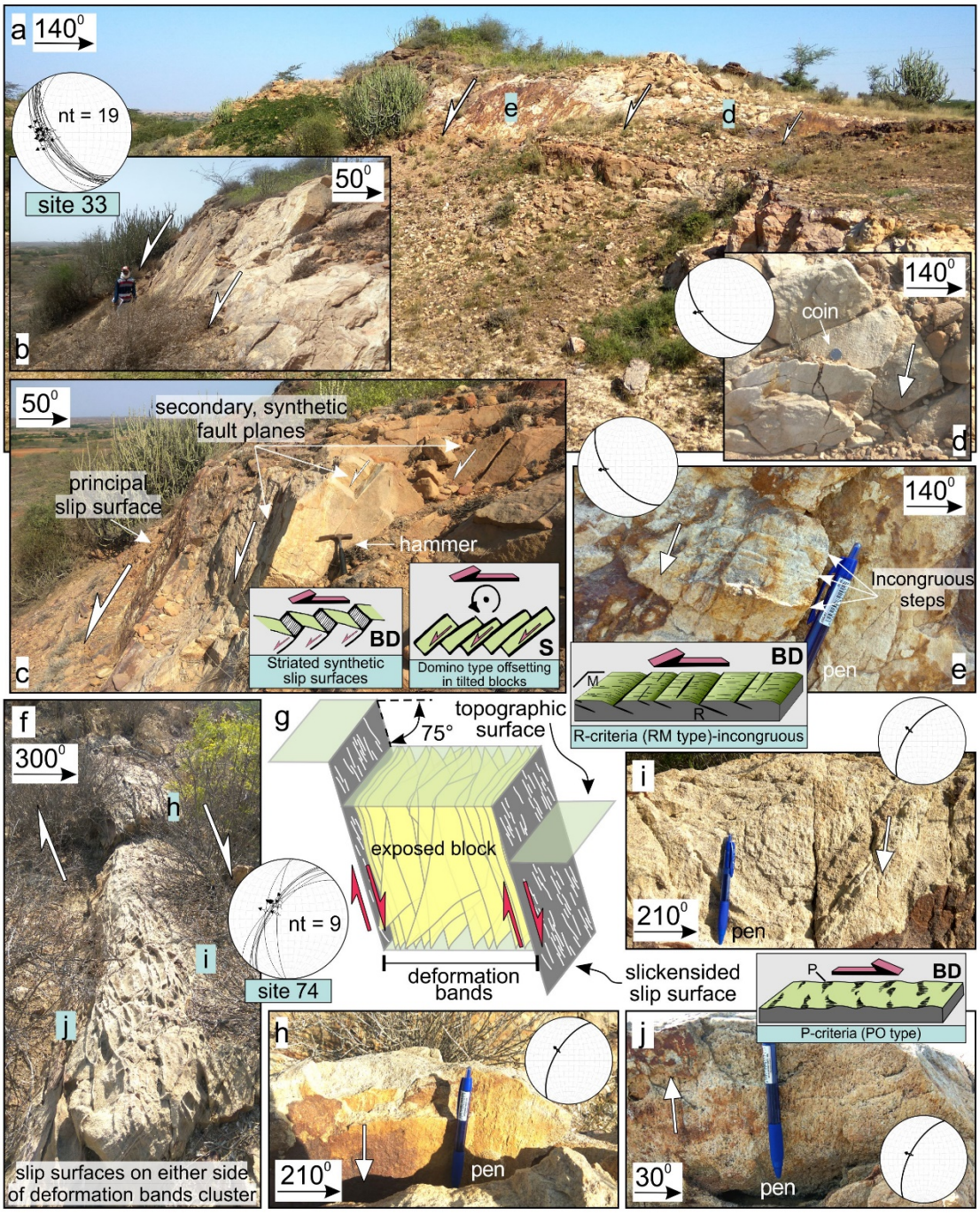

Fig. 7.3. (a)-(e) NW striking GUF with normal slip exposed at site 33 (sector 1) and (f)-(j) NNE striking cluster of deformation bands exposed along with the striated slip surfaces on both sides, at site 74 (sector 1). See the structural map in Fig. 7.2 for site location. (a) Panoramic-view of the GUF. d and e denote location of close-ups shown in Figs. (d) and (e). (b) NW looking outcrop-view of the GUF. Height of the person is 188 cm as a scale. (c) Close-view of the exposed footwall shows both the principal slip plane and synthetic, striated slip planes. Length of hammer: 30 cm as scale. (d) and (e) NE looking, close-ups of striated fault plane (attitude: 140° strike, 230° dip direction, 57° dip and lineations attitude: 113° and 110° rake, 48° and 55° plunge, 189° and 203° azimuth). (f) Outcrop-view of deformation bands cluster. h to j show location of close-ups of striated slip planes. (g) The block diagram shows cluster of deformation bands (variably dipping yellow planes) bounded on either sides by striated slip planes (grey colored striated planes). The green horizontal planes show level of topographic surfaces. (h)-(j) The striated fault plane (attitude: 210-230° strike, 300-320° dip direction, 60-70° dip amount and lineations attitude: 93-99° rake, 60-69° plunge, 313-339° azimuth). 13.5 cm long pen as scale in Figs. (e), (h)-(j). Inset sketches: block diagram (BD) of striated synthetic slip surfaces, sectional- (s-) view of domino-type offsetting in tilted blocks in Fig. (c) – modified after fig. 1 of Doblas (1998); BD of RM structures in Fig. (e), PO structures in Fig. (j) – modified after figs. 1e and 1f of Petit (1987). The white arrows indicate movement of the missing block.

Strike of the KMF changes from NW-W where the GUF meets the KMF. Thus, GUF at site 33 (sector 1) acts as a transverse fault and is responsible for the change in strike of the KMF. Because of the tectonic movement along GUF, ENE striking, ~3.3 km long, linear ridge got truncated abruptly on its western end, from where the fault passes and generated a valley locally in the hangingwall side of the fault (Fig. 7.3a).

Slip-sense is determined by observing the following kinematic indicators: *(i)* development of the secondary, synthetic, striated fault planes; bounding the titled blocks in the footwall indicate domino-style deformation. Along with the principal slip surface, secondary slip planes have experienced downslope movement (Fig. 7.3c) (Doblas, 1998), and *(ii)* incongruous fracture steps have been worn by friction during fault movement. These are associated with the negative smoothness criterion (Angelier, 1994) and suggest normal slip. They are arranged in the direction opposite to movement of missing hangingwall and near-perpendicular to striations (Fig. 7.3e). The steps are of RM-type described by Petit (1987) wherein the main fault plane (/mean fault plane/M surface) is fully striated. R fractures are clearly visible at the tip of dihedron formed by intersection of R and M surfaces. It is noteworthy that the R fractures are closely-spaced, exposed only in a small patch and dipping at low-angle in the M surface.

Paleostress analysis results indicate that the GUF at site 33 (sector 1) is showing oblique-slip with dominant normal dip-slip and minor dextral strike-slip components, related to pure extensional stress regime with N71° striking S_{hmin} (Appendix-B).

SECTOR 2

The investigated sites in sector 2 show dominance of NW-NNW striking VF and GUF, NE striking unnamed faults which terminate against the VF and GUF, and few E striking, high-angle, oblique-slip faults (Fig. 7.4).

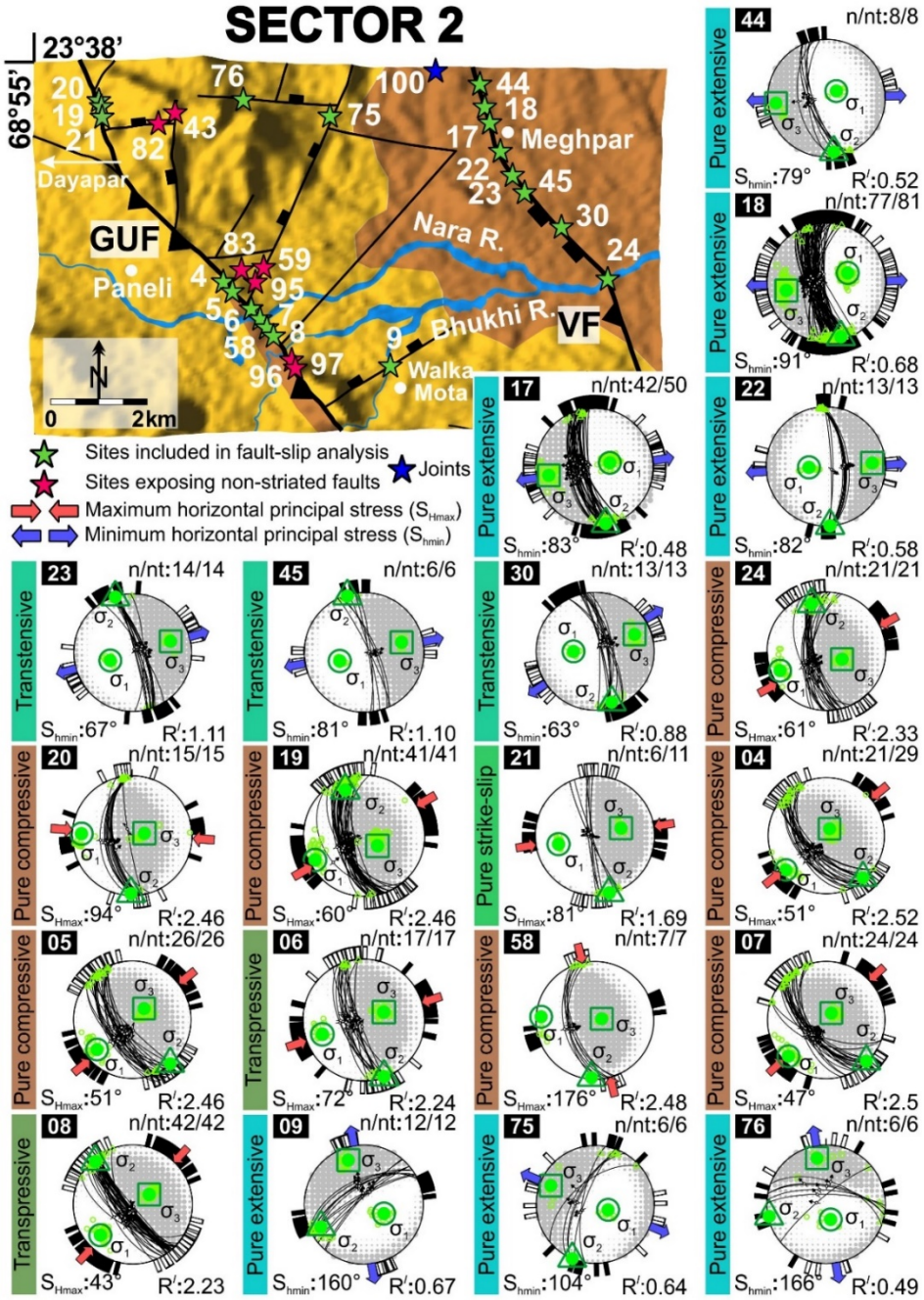

Fig. 7.4. Structural map of sector 2 (location shown in the geological map of study area in Fig. 7.1). Follow Fig. 7.2 caption for interpretation of map and paleostress tensors deduced by Win_Tensor (Delvaux and Sperner, 2003).

Vigodi Fault (VF) with changing slip-sense

South of the Haroda Pluton, the SW dipping VF is exposed in Jhuran sandstone at sites 44, 18 and 17 (sector 2) in the form of ~1.5 km long, narrow, asymmetric, ~10 m high hill (Fig. 7.5). ~10 m elevation of the hill is the estimate of surficial throw along the fault. The surficial throw abruptly decreases at sites 22, 23, 45 and 30 (sector 2) where 30-50 cm high striated fault plane crops out from the surrounding flat soil surface.

Sites 44 and 18 (sector 2) are located SSE of the Haroda Pluton (Fig. 7.5). The kinematic indicators observed are as follows – *(i)* Secondary, synthetic, striated slip surfaces exposed along with the principal slip surface (main fault plane) in the footwall (Figs. 7.5a, g). Their structural attitude is roughly the same as principal slip surface and suggest domino-style deformation of titled blocks. All the secondary slip surfaces have experienced normal slip. Eight and 81 fault-slip data are recorded from the principal slip surface as well as from the secondary slip surfaces at sites 44 and 18 respectively. *(ii)* Secondary quartz slickenfibers consistently terminate downslope against the mineral steps (Fig. 7.5b). The mineral risers step down consistently indicating downslope movement of the missing hangingwall. *(iii)* Crisscrossing, secondary, synthetic and antithetic fractures can be observed (Fig. 7.5c). The synthetic fracture shows normal drag fold with round hinge and of dissimilar geometries. Normal drag is inferred as the structural elements in the upthrown side have dragged down. The antithetic fracture does not show any displacement and drag. *(iv)* Knobby asymmetric elevations on the striated fault plane suggest downslope movement of the missing hangingwall (Figs. 7.5d, e). *(v)* PT structure of Petit (1987) (Figs. 7.5b, f) are found useful in deciphering normal slip of the VF. M surface is incompletely striated. The striated P surfaces on stoss side of PT structures are prominently developed and T surfaces are dipping into the M surface at a low angle (Fig. 7.5b). P surfaces are more developed and striated in Fig. 7.5b than in Fig. 7.5f. The intersection of P and T surfaces at the lee side of PT structures has been broken and forms many small steps.

At sites 22, 23, 30 and 45 (sector 2, Fig. 7.4), normal slip along the NE dipping, ~30-50 cm high, VF has been inferred by observing risers stepping up indicating

upward movement of the missing footwall. N-NE striking sub-vertical joints are exposed in Jhuran sandstone at site 100.

The paleostress analysis results indicate that, in the middle segment of the VF, south of Haroda Pluton for about 5 km, there has been a shift in stress regime from pure compressive to pure extensive along the strike of the VF. S_{Hmax} strikes N147°-N178° and S_{hmin} strikes N077°-N090° indicating ~N-S compression with R' ranging from 0.48-1.11 (Appendix-B).

Gugriana Fault (GUF) with reverse slip

In sector 2, the GUF is exposed at sites 4, 5, 6, 58, 7, 8 and acts as a lithotectonic contact between Jhuran shale in the hangingwall (partially exposed) and Bhuj sandstone (well-exposed) in the footwall (Fig. 7.4). NNW striking GUF exposed at sites 19, 20 and 21 in Bhuj sandstone is devoid of Jhuran sandstone/shale in the hangingwall (Fig. 7.4). In sector 2, the slip-sense along the GUF changes to reverse dip-slip. This is in contrast to the manifestation of GUF at site 33 (~13 km NW of site 20) in sector 1 where it shows oblique-slip with dominant normal dip-slip and minor dextral strike-slip components.

~1 m high fault plane exposed in Bhuj sandstone crops out from the surrounding flat soil surface at site 19 (Sector 2; Figs. 7.6a-f). The kinematic indicators observed are as follows – *(i)* The risers of asymmetric cavities found on the striated fault surface neither face up-slope nor down-slope in order to determine the slip-sense (Fig. 7.6d). *(ii)* Parallel to sub-parallel tension gashes oriented parallel/oblique to striations in plan-view of the fault can be observed (Fig. 7.6e). The slip-sense can only be inferred when tension gashes are observed in sectional-view (s-view as shown in the inset sketch, fig. 1 (1/FR: Fractures) of Doblas, 1998). Any uniformity in dip of tension gashes was not observed in s-view and therefore, whether the tension gashes dip in the direction of movement of missing block, could not be determined. *(iii)* Reverse slip is inferred from RO structures of Petit (1987) (Fig. 7.6f). The tiny R shears dipping at low-angle into the fault plane and distance between them is very small and regular. M surface appears to be serrated in cross-sectional view.

Site 7 (sector 2) exposes the GUF in the NE flowing tributary of the Khari river (Figs. 7.4, 7.6g-j). The river here has taken a circular rhythmic turn due to deflection in river course on account of faulting. The GUF shows reverse slip as the older Jhuran shale in the hangingwall has come in contact with the younger Bhuj sandstone in the

footwall (Figs. 7.6g, h). The striated fault plane has been affected by conjugate set of tensile fractures (mode I) ranging in dimension up to tens of centimeters (Fig. 7.6i). Fractures could not be utilized to determine the slip-sense. Reverse slip is supported by positive smoothness criterion. NNW trending GUF exposed in highly fractured Bhuj sandstone, at site 20 (sector 2), ~3.2 km east of Dayapar. ~1.5 m high GUF is cropping out of the surrounding low-lying soil surface.

The fault-slip analysis results indicate that the GUF with reverse slip in sector 2 is related to pure compressive to transpressive stress regime with $R' \approx 2.50$ and NE-E directed compression (Appendix-B).

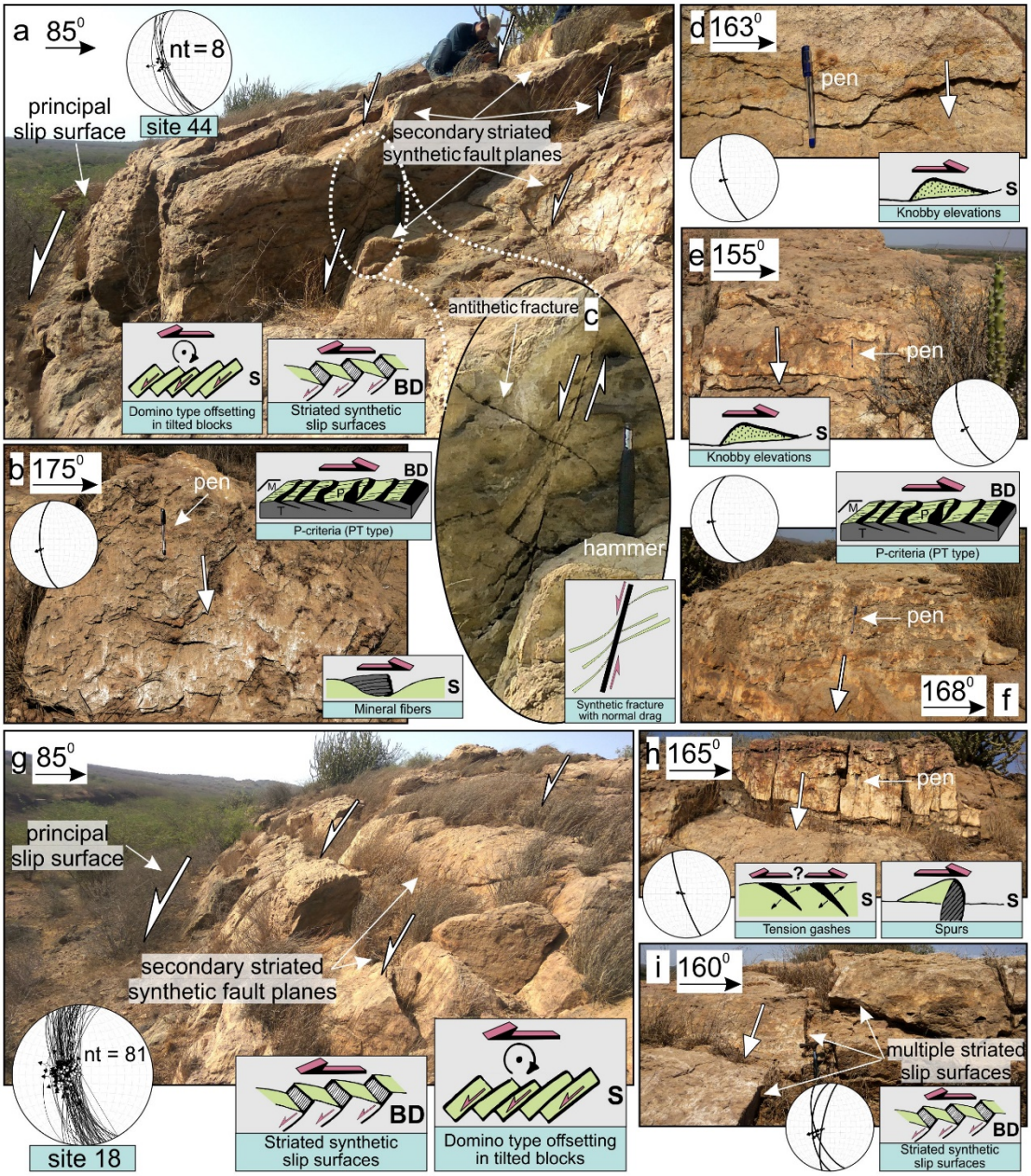

Fig. 7.5. NNW striking VF with normal slip exposed (a)-(f) at site 44 (sector 2) and (g)-(i) at site 18 (sector 2). See the structural map in Fig. 7.4 for site location. (a) Multiple, synthetic, striated, secondary slip planes exposed in footwall along with the major slip surface. (b) East looking, close-view of striated fault plane (attitude: 175° strike, 265° dip direction, 64° dip and attitude of lineations: 83° rake, 63° plunge, 249° azimuth). Mineral steps consistently facing down-slope indicate down-slope movement of the missing block. (c) North looking, close-view of a portion of footwall shown as dotted circle in Fig. (a). Length of hammer is 30 cm as scale. (d)-(f) East looking, close-view of the striated fault plane (attitude: 155-168° strike, 245-258° dip direction, 48-71° dip and attitude of lineations: 88-94° rake, 48-71° plunge, 239-264° azimuth). (g) North looking, fault-parallel view of VF. (h) ENE looking, close-view of the striated fault plane (attitude: 161° strike, 251° dip direction, 82° dip and attitude of lineations: 94° rake, 81° plunge, 278° azimuth). The striated fault plane is intensely affected by sub-parallel tension gashes. (i) ENE looking, close-view of multiple striated slip planes (average attitude: 179° strike, 269° dip direction, 57° dip and average attitude of lineations: 80° rake, 56° plunge, 251° azimuth). Inset sketches: sectional- (s-) view of domino-type offsetting in tilted blocks, block diagram (BD) of (sub)-parallel striated, synthetic slip surfaces in Figs. (a), (g) and (i); s-view of mineral fibers in Fig. (b); s-view of knobby elevations in Figs. (d) and (e); s-view of tension gashes and spurs in Fig. (h) – modified after fig. 1 of Doblas, (1998). S-view of synthetic fracture with normal drag in Fig. (c). BD of fractures with PT structures in Figs. (b) and (f) – modified after fig. 1 of Petit (1987). 13.5 cm long pen as scale in Figs. (b), (d)-(f) and (h). The white arrows indicate the downward motion of missing hangingwall.

SECTOR 3

In sector 3, NW striking GUF, and NE, E and SE striking unnamed faults are exposed in Jhuran and Bhuj sandstones (Fig. 7.7). NW striking VF and NNW striking WVF both serving as lithotectonic contact between Jhuran and Bhuj sandstone are also exposed.

Vigodi Fault (VF) with reverse slip

In sector 3, NW striking VF exposed in Bhuj sandstone is investigated at sites 27, 28, 87, 36 and 37 (Fig. 7.7).

Site 27 (sector 3) exposes NW striking, ~3 m high, striated VF (Figs. 7.8a-e). Site 28 (sector 3) is located ~400 m SE of site 27 (Fig. 7.7). The striated fault plane exposes ridge-in-groove lineations (/corrugations). Linear, pipe-shaped gouging grain grooves developed by down-dip movement of protruding grains/clasts indicate upslope movement of the hangingwall (Fig. 7.8b). Also note the conjugate set of fractures formed on faulted surface.

Carrot-shaped tool marks generated due to gouging effect of the quartz grains dragged down-dip are also visible with the naked eye (Fig. 7.8c). Acute angle or concavity of the kinematic indicator lies in the upslope motion of the hangingwall indicating reverse slip.

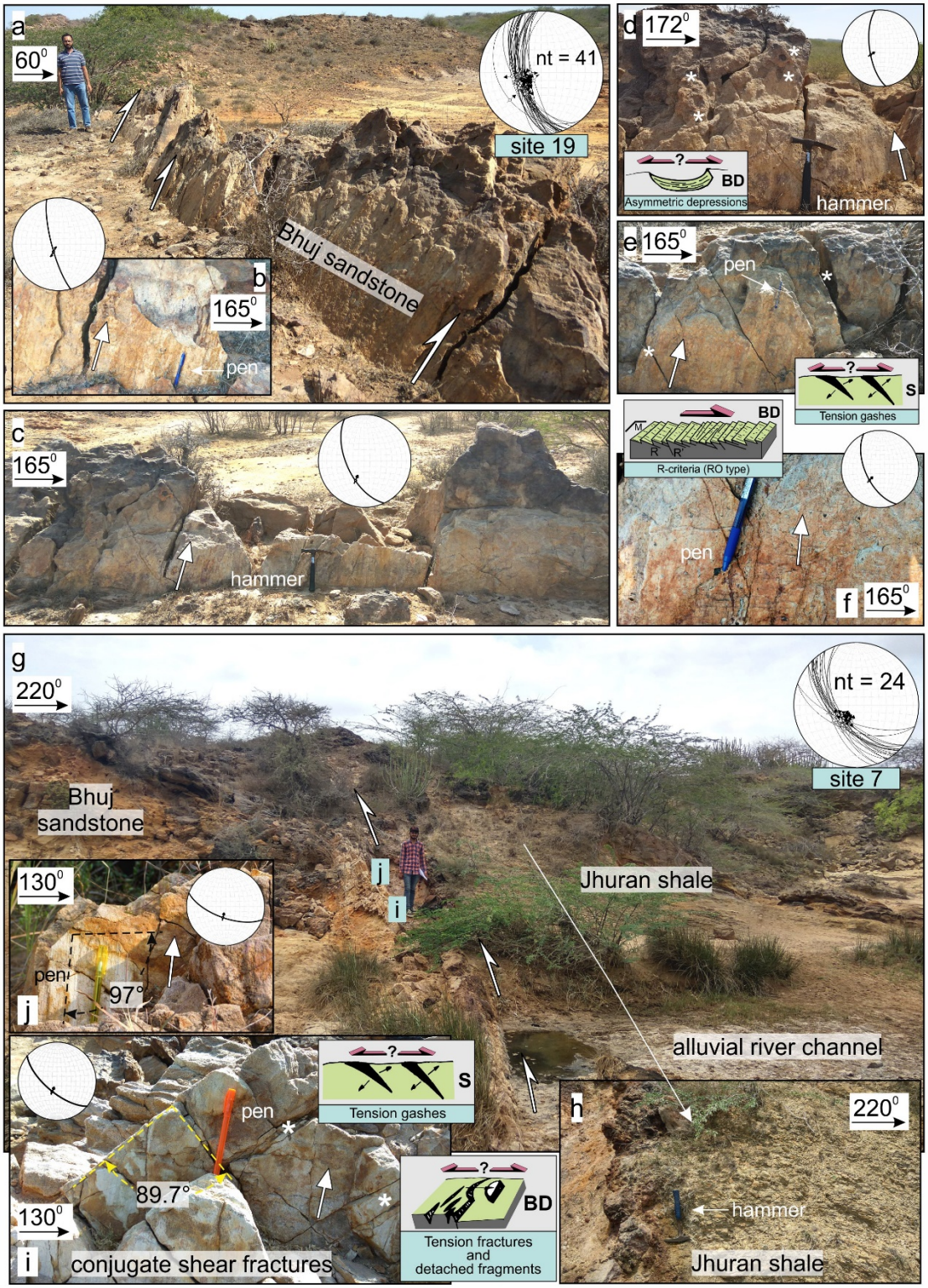

Fig. 7.6. (a)-(f) NNW striking GUF with reverse slip exposed at site 19 (sector 2) and (g)-(j) NW striking GUF with reverse slip exposed in the cliff section of an alluvial river channel of the NE flowing Khari river, at site 7 (sector 2). See the structural map in Fig. 7.4 for site location. (a) Outcrop-view of the GUF. Height of the person is 178 cm as scale. (b)-(f) The fault plane (attitude: 155-172° strike, 245-262° dip direction, 59-78° dip) with striations (101-114° rake, 52-76° plunge and 267-288° azimuth). (g) Outcrop-view of the GUF. Height of the person is 188 cm as scale. i and j denote the location of close-ups shown in Figs. (i) and (j). (h) Close-view of the Jhuran shale lithology lying on the hangingwall of SW dipping GUF. 30 cm long hammer as scale. (i) and (j) Essentially dip-slip striations (96° and 97° rake, 66° and 60° plunge, 205° and 193° azimuth) developed on a fault plane (attitude: 130° and 110° strike, 220° and 200° dip direction, 67° and 66° dip). A 30 cm long hammer as scale in Figs. (c), (d), (h), and 13.5 cm long pen as a scale in Figs. (b), (e), (f), (i) and (j). Inset sketches: block diagram (BD) of asymmetric depressions in Fig. (d), BD of detached fragments marked by white asterisk in Fig. (i), sectional- (s-) view of tension gashes in Figs. (e) and (i) – reproduced from fig. 1 of Doblas (1998). BD of fractures with RO structures in Fig. (f) – reproduced from fig. 1 of Petit (1987). The white arrows indicate the upward motion of missing hangingwall.

The only exposure of striated fault plane (20° rake) denoting sinistral strike-slip motion is also observed, which pre-dates the reverse slip (Fig. 7.8e). Due to unavailability of more such fault planes with strike-slip striations, it is not included in the analysis.

At site 87 (sector 3), the fault crosses the NE flowing Makdawali river (Figs. 7.7, 7.8f, g). The SW dipping, dense cluster of deformation bands along with the striated, principal slip surface occur in the fault damage zone (Fig. 7.8f). The striated fault plane shows shear fractures (PT-type) near-perpendicular to the orientation of striations (Fig. 7.8g). See Fig. 7.5b description for details regarding morphology of fractures following the PT-criteria of Petit (1987).

~3.5 km NE of site 87 in sector 3, another NNW striking fault is encountered cross-cutting the NE flowing Makdawali river (Fig. 7.8h). The fault exposes multiple generations of striations in which the dip-slip striations clearly seem to truncate the striations denoting strike-slip motion. The fault is not included in paleostress analysis due to insufficient number of fault-slip data (nt = 2). The fault-slip analysis results indicate that the VF with reverse slip exposed in sector 3 is related to pure compressive stress regime with R' ranging 1.93-2.52 and NNE-NE directed compression (Appendix-B).

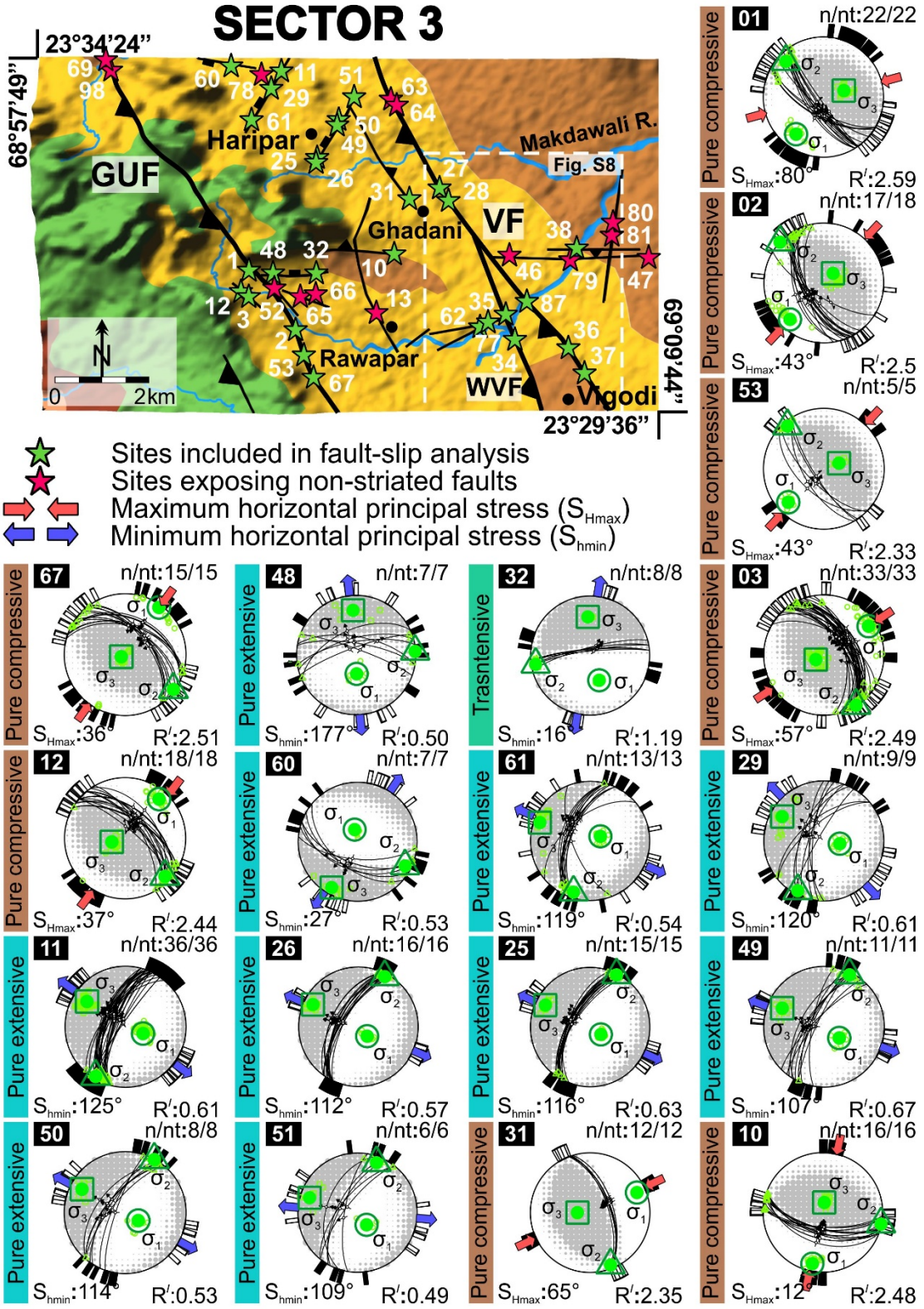

Fig. 7.7. Structural map of sector 3 (location shown in the geological map of study area in Fig. 7.1). Follow Fig. 7.2 caption for interpretation of map and paleostress tensors deduced by Win_Tensor (Delvaux and Sperner, 2003).

West Vigodi Fault (WVF) with reverse slip

At sites 34 and 35 (sector 3), the SW dipping WVF is exposed in Bhuj sandstone at one of the cliff section of NE flowing Makdawali river (Figs. 7.7, 7.9a-d). The Makdawali river has been deflected, where the fault crosses the river. The two E and NE flowing tributaries meet where the fault passes through, the river then flows towards NE. The multiple, synthetic, striated slip planes indicate upward movement of the missing hangingwall (Fig. 7.9d). The rake of lineations goes up to ~135° indicating sinistral strike-slip component is also involved along with the reverse slip. The fault-slip analysis results indicate that the WVF is related to pure compressive stress regime with NE oriented compression (Appendix-B).

Gugriana Fault (GUF) with reverse slip

The SW dipping, striated GUF exposed in Bhuj sandstone is investigated at sites 1, 2, 53 and 67 (Fig. 7.7).

At site 67 (sector 3), the NE striking GUF is exposed in Bhuj sandstone (Figs. 7.7, 7.9e-j). SSE of site 2, the dip direction of NW striking GUF changes from SW and dip towards NE (Figs. 7.9e-j). The slip-sense has been inferred by observing the following kinematic indicators – *(i)* asymmetric cavities (Figs. 7.9f, g) and *(ii)* linear, pipe-shaped grooves generated due to gouging effect of grains (Figs. 7.9h, i) indicate upward movement of the missing hangingwall. *(iii)* P fractures oblique to the orientation of striations are also observed (Fig. 7.9j). The fault-slip analysis results indicate that the GUF exposed in sector 3 is related to pure compressive stress regime with $R' \approx 2.5$ and NE oriented compression (Appendix-B).

(i) WSW striking deformation band fault at site 62 shows normal slip and NNW striking slipped deformation band at site 77 is also showing normal slip and, *(ii)* NW striking deformation band fault with reverse slip is exposed at site 12.

SECTOR 4

NW striking parallel NF, GUF, NKHF, VF; and NNW striking KF and WVF are exposed in sector 4 (Fig. 7.10). The NKHF and KF, where the former and northern segment of the later serve as lithotectonic contact between Jhuran and Bhuj sandstone. The NKHF is non-striated and is therefore, not included in the paleostress analysis.

Gugriana Fault (GUF) with reverse slip

The southernmost extremity of NNW-NW striking GUF appears in sector 4. The fault is exposed for ~5 km in Bhuj sandstone with subsidiary, local occurrence of shale lithology in fault damage zone at sites 39, 40 and 41 (Fig. 7.10). At site 41 (sector 4), GUF is exposed ~300 m east of the NNW striking asymmetrical hill range with steep eastward and gentler westward slope (Fig. 7.11). Locally, the fault appears to be of having curved geometry with strike ranging between N140°-N190° E (Fig. 7.11a). The striated slip surfaces are found on both the sides of the positive relief structure. Carrot-shaped (Figs. 7.11c, g) and pipe-shaped gouging grain grooves (Figs. 7.11e, g) are formed due to plucking effect of upward moving grains during fault motion.

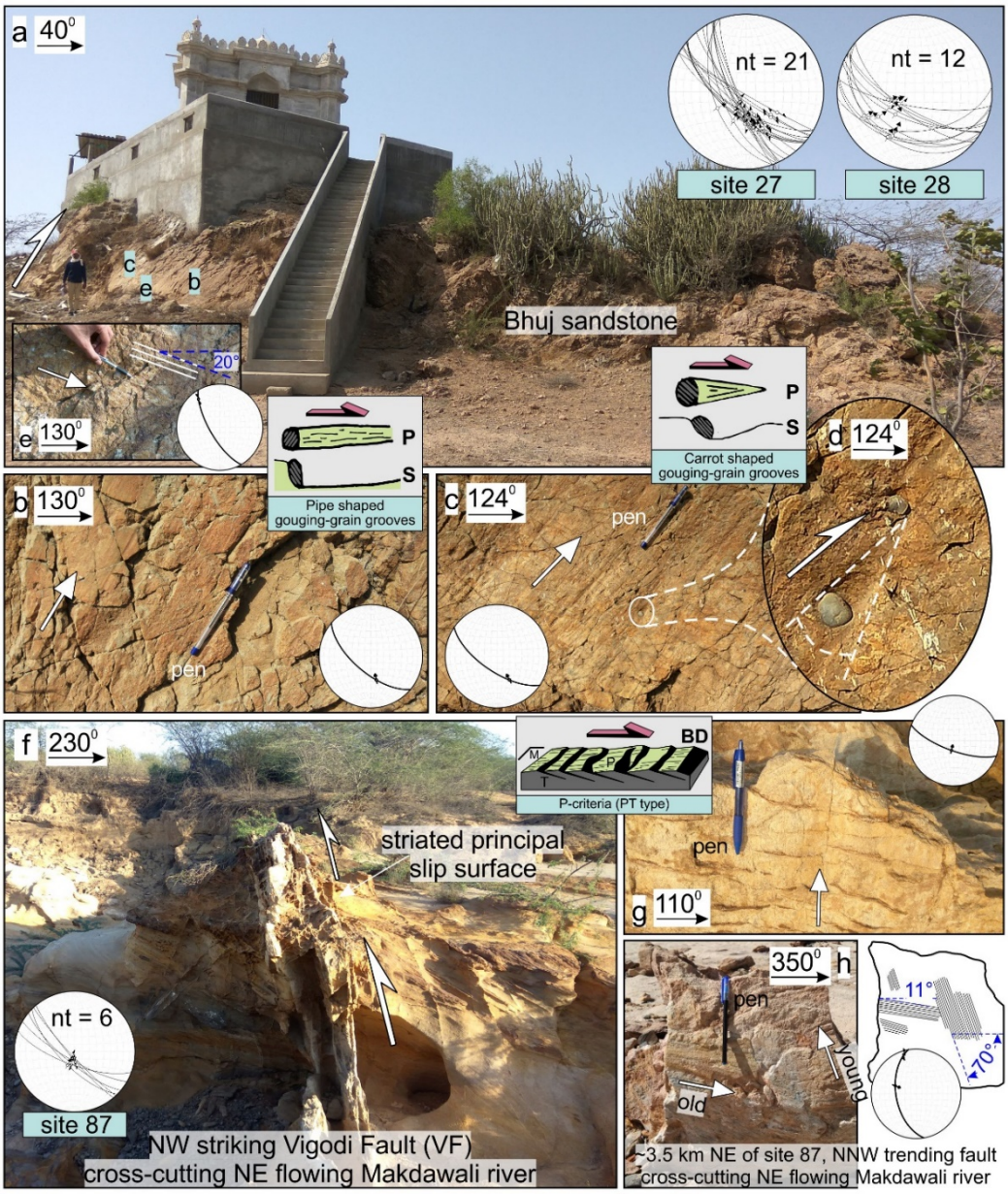

Fig. 7.8. (a)-(e) NW striking VF with reverse slip at site 27 (sector 3), (f) and (g) NW striking VF with reverse slip cross-cutting NE flowing Makdawali river, at site 87 (sector 3). Se the structural map in Fig. 7.7 for site location. (a) Outcrop-view of the VF. Height of the person is 188 cm as scale. (b) and (c) The striated fault plane (attitude: 130° and 124° strike, 220° and 214° dip direction, 64° and 66° dip, attitude of lineations: 120° and 127° rake, 51° plunge and 167° and 152° azimuth). In close-view, pipe-shaped linear grooves can be observed in Fig. (b). Carrot-shaped grooves can be observed due to dragging effect of grains. (d) Close-view of carrot-shaped markings shown in Fig. (c). (e) The striated fault plane (attitude: 150° strike, 240° dip direction, 71° dip, attitude of lineations: 20° rake, 19° plunge, 323° azimuth). Location of Figs. (b), (c) and (e) are shown in Fig. (a). (g) The fault plane (attitude: 110° strike, 200° dip direction, 72° dip) with striations (92° rake, 72° plunge, 194° azimuth). (h) Close-up of the fault plane (attitude: 350° strike, 260° dip direction, 53° dip) with two generations of striations (70° and 11° rake, 49° and 09° plunge, 291° and 343° azimuth). 13.8 cm long pen as scale in Figs. (b), (c), (e), (g) and (h). Inset sketches: plane- (p-) and sectional- (s-) view of pipe-shaped and carrot-shaped gouging-grain grooves in Figs. (b) and (c) respectively – modified after fig. 1 of Doblas (1998). Block diagram (BD) of PT type fractures in Fig. (g) – modified after fig. 1f of Petit (1987). The white arrows indicate the motion of missing hangingwall.

This indicates a downward movement of the missing footwall. See Fig. 7.8 description for details regarding morphology of carrot-shaped and pipe-shaped gouging grain grooves of Doblas (1998). RO-type fractures in Fig. 7.11d also suggest downward motion of the missing footwall.

The fault-slip analysis results indicate that the GUF with reverse slip exposed in sector 4 is related to pure compressive to transpressive stress regime with R' ranging 2.20-2.45 and NE oriented compression (Appendix-B).

Netra Fault (NF) and Khirasra Fault (KF) with reverse slip

Knobby, asymmetric elevations sloping upward observed on striated fault plane indicate upward movement of the missing hangingwall thereby suggesting reverse slip along the NF. The NNW striking KF, which is a branch of GUF, is exposed at sites 42 and 57 (sector 4). At both the sites, the fault is exposed on top of a narrow, linear NNW striking fault-controlled hill. Smooth-rough criteria worked well as friction felt downslope suggesting upward movement of the missing hangingwall thereby indicating reverse slip.

The VF shows reverse dip-slip in sectors 1, 3 and 4, where the hangingwall on SW side has come up (e.g., Fig. 7.8). However, in sector 2, south of the Haroda pluton,

the slip-sense alters to normal dip-slip (e.g., Fig. 7.5). Also, in sector 2, the dip direction of VF changes with *(i)* SW dipping fault plane in the northern segment (Fig. 7.5) which rotates to *(ii)* NE dipping fault plane in the southern segment with abrupt decrease in throw.

The fault-slip analysis results indicate that the NF and KF with reverse slip are related to pure compressive stress regime with $R^{/}$ ranging 2.09-2.51 and NE oriented compression (Appendix-B).

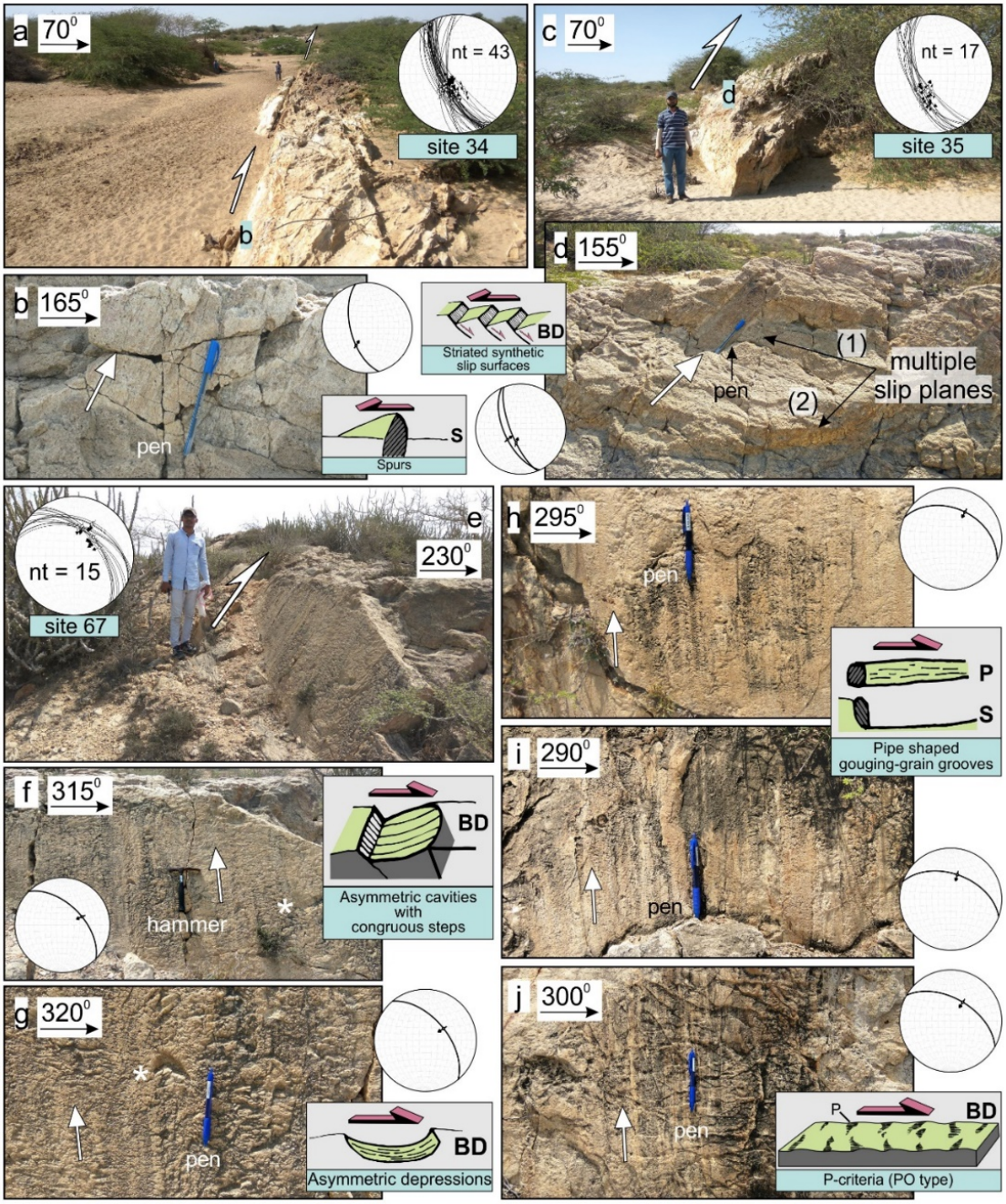

Fig. 7.9. (a)-(d) NNW striking WVF with reverse slip at sites 34 and 35 (sector 3), and (e)-(j) NW striking GUF with reverse slip exposed at site 67 (sector 3). See the structural map in Fig. 7.7 for site location. (a) WVF exposed at one of the cliff section of the NE flowing Makdawali river. (b) Close-view of the striated fault plane (attitude: 165° strike, 255° dip direction and 60° dip and attitude of lineations: 115° rake, 52° plunge and 212° azimuth). (c) Fault-parallel view of WVF. Height of the person is 178 cm as scale. (d) Close-view of the two striated fault planes of the same generation. Plane (1) and (2): 158° and 155° strike, 248° and 245° dip direction, 72° and 60° dip, 110° and 97° rake, 63° and 59° plunge, 198° and 231° azimuth. Location of Figs. (b) and (d) are shown in Figs. (a) and (c) respectively. (e) Outcrop-view of the GUF. Height of the person is 188 cm as scale. (f)-(j) The striated fault plane (attitude: 290-320° strike, 25-50° dip direction, 28-55° dip and attitude of lineations: 77-93° rake, 49-55° plunge, 15-67° azimuth). Asymmetric cavity with congruous steps and asymmetric depression facing upslope marked by white asterisk in Figs. (f) and (g) respectively. Figs. (h) and (i) show cm long, linear, pipe-shaped gouging-grains leaving thick black grooves due to their upslope movement on the fault plane. P fractures generated almost perpendicular to striations orientation can be observed in Fig. (j). Inset sketches: sectional- (s-) view of mineral steps in Fig. (b), block diagram (BD) of striated synthetic slip surfaces in Fig. (d), BD of asymmetric cavities with congruous steps in Fig. (f), asymmetric depression in Fig. (g), plane- (p-) and s-view of pipe-shaped gouging-grain grooves in Figs. (h) and (i) – modified after fig. 1 of Doblas (1998). BD of P fractures in Fig. (f) – modified after fig. 1f of Petit (1987). 13.8 cm long pen as scale in Figs. (b), (d), (g)-(j). 30 cm long hammer as scale in Fig. (f). The white arrows indicate the upward motion of missing hangingwall.

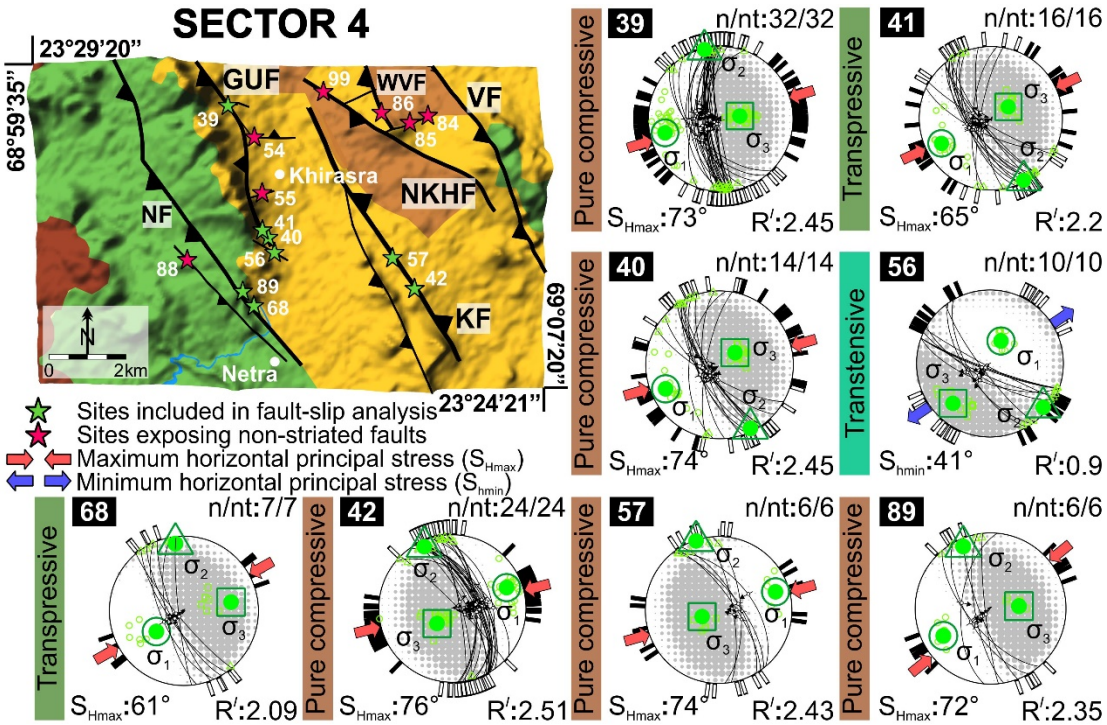

Fig. 7.10. Structural map of sector 4 (location shown in the geological map of study area in Fig. 7.1). Follow Fig. 7.2 caption for interpretation of map and paleostress tensors deduced by Win_Tensor (Delvaux and Sperner, 2003).

However, slip-sense remains the same i.e., normal dip-slip with *(i)* missing hangingwall on SW side of the fault plane has moved down with respect to the exposed footwall in the case of SW dipping VF whereas *(ii)* missing footwall on SW side has moved up and eroded away with respect to the exposed hangingwall in the case of NE dipping VF. NNW striking WVF, bifurcates from the NW striking VF along its northern extremity (in sector 3; Fig. 7.7) and ends up against the NW striking NKHF along its southern extremity (in sector 4; Fig. 7.10). It shows oblique-slip with reverse dip-slip and sinistral strike-slip components (Figs. 7.9a-d).

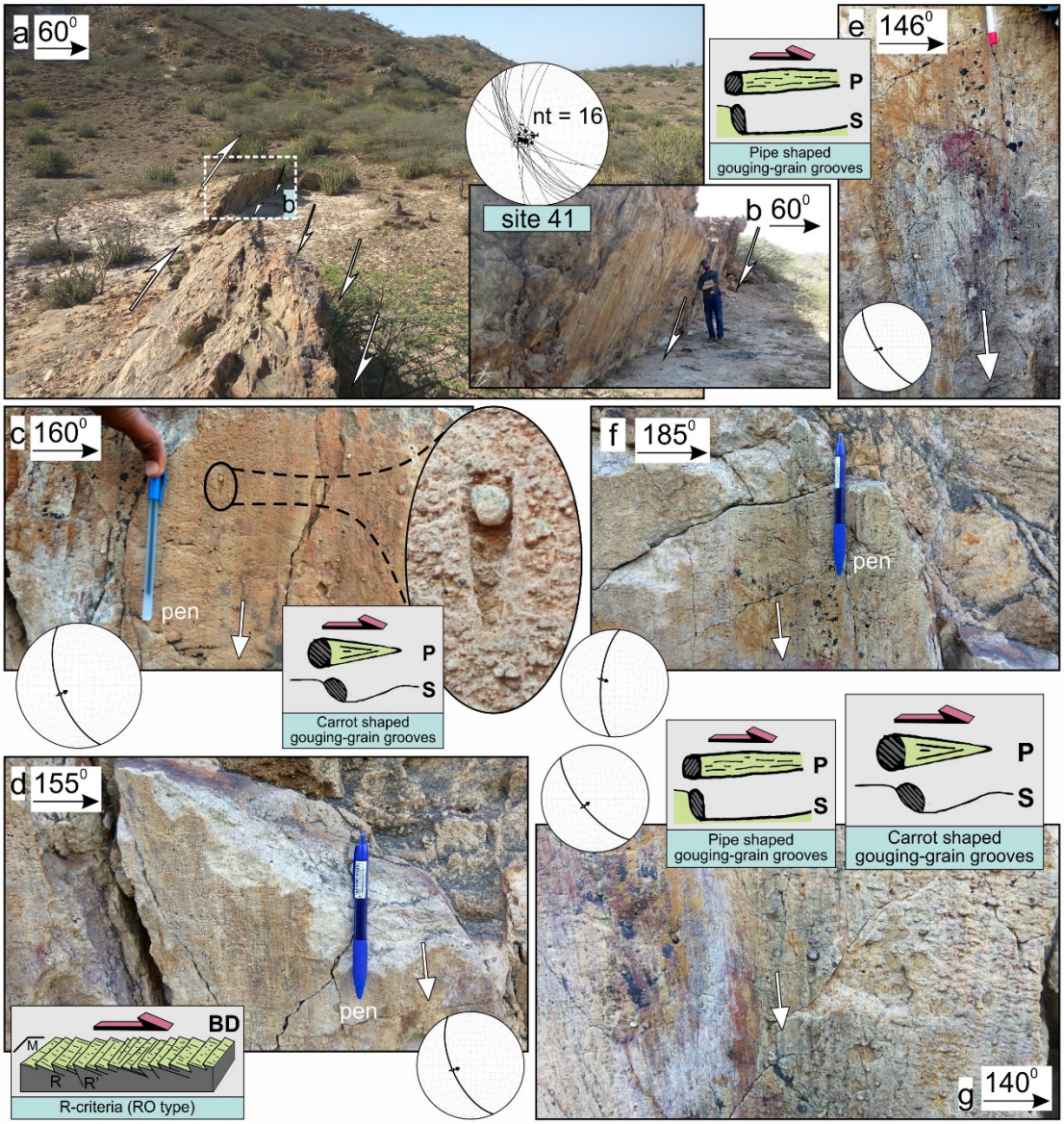

Fig. 7.11. (a) Panoramic view of NNW striking GUF with reverse slip exposed at site 41 (sector 4, see the structural map in Fig. 7.10 for site location). (b) NNW looking, fault-parallel view of the GUF. Height of the person is 178 cm as scale. Location of Fig. (b) is shown as white square in Fig. (a). (c)-(g) Close-view of striated fault plane (attitude: 146-185° strike, 250-275° dip direction, 63-72° dip and lineations attitude: 84-92° rake, 63-71° plunge, 246-286° azimuth). Inset sketches: plane- (p-) and sectional- (s-) view of carrot-shaped gouging-grain grooves in Figs. (c), (g) and pipe-shaped gouging-grain grooves in Figs. (e), (g) – modified after fig. 1 of Doblas (1998). Block Diagram (BD) of fractures with RO structures in Fig. (d) – reproduced from fig. 1 of Petit (1987). 13.5 cm long pen as scale in Figs. (c)-(g). The white arrows indicate the motion of missing block.

Comparing the exposure of GUF in all the four sectors, it is observed that SW-WSW dipping footwall is exposed in sectors 1, 2 and 3 while the hangingwall is missing (Figs. 7.3a-e). Whereas in sector 4, the SW-WSW dipping hangingwall is exposed and footwall is missing (Fig. 7.11). The GUF in its NW extremity, in the vicinity of KMF, is characterized by oblique-slip with dominant normal dip-slip and minor dextral strike-slip components (site 33 in sector 1). While in rest of the sectors, GUF shows reverse slip. Thus, the GUF shows along-strike change in slip-sense. Furthermore, change in the orientation of slickenside lineations along the strike of GUF has been observed. At its northernmost extremity, GUF at site 33 (sector 1) exposes striations with rake ranging 100-120° (measured with respect to N140° fault strike, Figs. 7.3d, e), while at its southernmost extremity, at site 41 (sector 4), GUF shows striations with rake 80-90° (measured with respect to N160° fault strike, Fig. 7.11). Putting it all together, it can be inferred that the GUF acted as a rotational fault (scissor/hinge fault) with no translational component involved with the axis of rotation lying perpendicular to the fault plane (e.g., models in Mukherjee and Tayade, 2019; Xu et al., 2011). The hangingwall on SW side of the GUF rotated anti-clockwise with respect to the fixed footwall lying on NE side. The anti-clockwise rotation of hangingwall involves downward movement at the northern extremity of GUF and upward movement at its southern extremity. The slip pattern observed along the GUF does not resemble the converging slip pattern along the normal faults described by Maniatis and Hampel (2008). The rotational fault (GUF) can be comparable with: the Alasehir basin in western Turkey (Oner and Dilek, 2013), Alhama de Murcia fault in eastern Betic Cordillera in southern Spain (Martinez-Diaz, 2002).

The NW striking NKHF (site 99) and NE striking KF (sites 42, 57) with reverse slip, which are the bifurcations of NNW striking GUF, are exposed in sector 4 (Fig. 7.10). The NW striking NF exposed in sector 4 (sites 68, 89) shows reverse slip (Figs. 7.10). The unnamed, cross-faults are exposed in each sector. The NNE and NE striking faults show normal slip (e.g., site 71) while the NW and E striking faults show reverse and/or normal slip.

The slickenside lineations are essentially straight, although Ghosh (1993) stated that purely translational faults seldom occur in nature. Curved stretching lineations are not observed on any of the fault planes. The synthetic shear has been observed in the exposed footwall/hangingwall in the sense that the development of secondary, synthetic, striated fault planes in the footwall indicate a domino-style deformation of the blocks and along with the principal slip surface, they have experienced downslope movement (e.g., Fig. 7.5). The carrot-shaped gouging-grain grooves developed *(i)* on the footwall of VF at site 27 (sector 3; Figs. 7.8c, d), their acute angle or concavity closes-up indicate the upward motion of missing hangingwall. *(ii)* Contrarily, at site 41 (sector 4) of the GUF, the carrot-shaped grooves are developed on the hangingwall with their acute angle close-down indicate the downward motion of missing footwall (Figs. 7.11c, g). All the studied sites are characterized by a population of homogeneous fault-slip data and therefore, no superposition/cross-cutting/truncation of multiple generations of striations is observed except a single outcrop (in sector 3, Fig. 7.8h). The NNW striking unnamed fault exposes dip-slip striations (rake ~70°) that truncate almost horizontal striations (rake ~11°). This indicates that reverse dip-slip post-dates the sinistral strike-slip motion.

Simón (2019) pointed out divergence in paleostress analysis results when different methods are applied in few cases. To avoid such a situation and to better constrain the paleostress analysis results, different methods were attempted and cross-checked the results across four different programmes. The same fault-slip data were tested with *(i)* different paleostress analysis procedures (e.g., FaultKin and SG2PS) and, *(ii)* with same procedures (e.g., RDM applied in Win_Tensor and T-Tecto). The paleostress tensors obtained through Win_Tensor and FaultKin are in good agreement with each other in terms of the trend of three principal stress axes (Appendix-B). The parameter D of T-Tecto is similar to stress ratio (R) defined by Delvaux et al. (1997) and suggest the stress regime for each site in proximity to each other. The derived paleostress tensors show steep plunge of one principal stress axis and sub-horizontal to

horizontal orientation of the other two indicating that the faults are non-Andersonian that have experienced changing stress fields temporally (Anderson, 1905; Yin and Ranalli, 1992). Since, faults-slip data were collected on the ground surface, stress variation with depth is beyond the scope of the present work.

The faults in the VGKNFS mark low cohesion. Therefore, they react to changing stress fields and record multiple movements. The segments of major faults with reverse slip are oriented perpendicular to the present-day compression. Therefore, they act as "weak" areas and may likely to reactivate in the compressive stress regime. Another factor that may influence the reactivation is frictional weakening of faults (review in Dutta and Mukherjee, 2019). Moreover, fault reactivation under ongoing compression is highly selective in the VGKNFS. In earlier studies (Sibson, 1995), it is inferred that only a few set of pre-existing normal faults or only individual segments of a single normal fault strand reactivate during inversion and form reverse faults. The same tectonic scheme of preferential reactivation is observed in the VGKNFS, where NW striking major faults are reactivated under NNE striking present-day compression, while NNE, NE and E striking unnamed faults are unfavorably oriented and remain passive to the inversion phase. The disorientation of unnamed, cross-faults in the sense that their NNE, NE and E strike is having non-perpendicular relationship with the current S_{Hmax} orientation. Furthermore, the entire length of major NW striking faults in the VGKNFS did not reactivate. This is in spite of the fact that they are oriented favorably to the current NNE oriented S_{Hmax}. Owing to selective reactivation, the individual segments of fault strand reactivated during inversion. Two cases are – *(i)* only ~5 km lateral stretch (in sector 2) in the middle segment of the VF remained non-responsive to inversion, and *(ii)* the GUF that acts as a scissor fault. Its NW extremity (in sector 1) remained silent during inversion and persisted normal slip, while the rest other parts have witnessed reverse slip (in sectors 2, 3, 4).